AERODYNAMIC AND THERMAL ENVIRONMENT OF A GAP UNDER HYPERSONIC FLIGHT

by

Haiming HUANG*, Jin GUO, and Guo HUANG

Institute of Engineering Mechanics, Beijing Jiaotong University, Beijing, China

Original scientific paper
https://doi.org/10.2298/TSCI1804753H

Accurate prediction of aerodynamic and thermal environment around a gap has a significant effect on the development of spacecraft. The implicit finite volume schemes are derived and programmed from Navier-Stokes equations. Taking the gap between thermal insulation tiles as an example, a numerical simulation is performed by the finite volume method to obtain the flow characteristic in a gap and then to analyze the heat transfer mechanism. The numerical results are consistent with the experimental ones, which prove the precision of the method used in this paper. Furthermore, the numerical results reveal that the heat convection plays a leading role in heat transfer around a gap.

Key words: *aerodynamic, finite volume method, gap flow, supersonic*

Introduction

In the flight of a high speed vehicle, the air around the vehicle is severely compressed, and the temperature of it increases to a sufficiently high level. In order to protect the high speed vehicle from the heat of the high temperature air, it is covered with the thermal protection system which consists of ceramic thermal insulation tiles [1-6]. Considering of the brittleness of ceramic tiles and the thermal expansion, a gap must be left between these tiles to avoid that ceramic tiles break against others. Thus, the high temperature air around the vehicle probably flows into the gap and then burns the vehicle. Besides, a gap most likely disturbs the flow field and causes the local heat effect [7]. In a gap, there are complicated vortex motions caused by the boundary-layer flow, so the gap flow is difficult to be studied by theory analyses. Up to now, the majority of researches about the gap flow have been done by NASA [8-14]. The NASA studied some influences on heat flux in a gap in experiments which were based on hypersonic wind tunnel tests and arc jet tests. The influences included geometrical shapes of a gap, width-to-depth of a gap, boundary-layer state (laminar or turbulent), *etc.* By these experimental studies, the value of pressure and heat flux in a gap were obtained, but the flow characteristic in a gap could not be shown, which brought difficulty to analyze the heat transfer mechanism. Fortunately, the flow characteristic can be obtained by a numerical simulation which makes up for lack of experiments. Regrettably, there has been no numerical simulation research about the gap flow exposed to a supersonic flow so far. In this paper, with the purpose to obtain the flow characteristic in a gap and analyze the heat transfer mechanism further, a numerical simulation was performed by the computer code that we have written.

* Corresponding author, e-mail: hmhuang@bjtu.edu.cn

Model

The 2-D physical model of a gap flow is built in fig. 1. The width and depth of the gap are L_∞ and $6L_\infty$, respectively, where L_∞ is defined as the characteristic length. The computational domain is shown in fig. 1(a). To conveniently describe the location of a point on the gap wall, the body-fitted curvilinear co-ordinate is established in fig. 1(b). The upstream corner is marked with O. Along the gap wall, the distance from the point O is *S*, and the total length of the gap wall is *L* ($L = 13L_\infty$). Hence, the location of a point on the gap wall can be described as *S/L* ranging from 0 to 1. At the boundary of the external flow field, far field boundary condition is utilized. At the wall, no-slip velocity and isothermal wall boundary condition with wall temperature 473.15 K are adopted. The parameters of the free stream are listed in tab. 1.

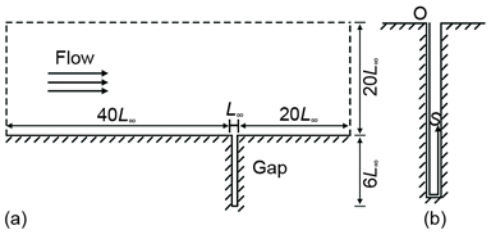

Figure 1. Physical model

Table 1. Parameters for free stream

Ma_∞	Re	T_∞
5.0	$5.6\cdot10^4$	473.15K

As the external flow outside a gap is at supersonic speed, it should be solved by the compressible Navier-Stokes equation. However, the flow in a gap is at low speed. The numerical algorithms for the compressible flow equation face difficulties for low Mach number conditions. In order to solve the nearly incompressible flow with numerical algorithms designed for compressible flows, the preconditioning technique proposed by Weiss *et al.* [14] is used in this paper. The 2-D integral compressible Navier-Stokes equation with a preconditioning matrix is described:

$$\int \frac{\partial \mathbf{U}}{\partial t} \mathrm{d}\Omega + \mathbf{Q}\boldsymbol{\Gamma}^{-1}\left(\oint_{\partial\Omega} \mathbf{F}\cdot\mathbf{n}\mathrm{d}s - \oint_{\partial\Omega} \mathbf{F}_v \cdot \mathbf{n}\mathrm{d}s \right) = 0 \tag{1}$$

where **U** is the vector of conservative variables, $\mathbf{F}\cdot\mathbf{n}$ and $\mathbf{F}_v\cdot\mathbf{n}$ represent the convective flux and the viscous flux, respectively, **n** – the unit normal vector of control volume faces. $\mathbf{F} = (\mathbf{F}_1, \mathbf{F}_2)$, $\mathbf{F}_v = (\mathbf{F}_{1v}, \mathbf{F}_{2v})$, $\mathbf{n} = (n_1, n_2)^T$. These quantities in eq. (1) are given by:

$$\mathbf{U} = \begin{pmatrix} \rho \\ \rho u \\ \rho v \\ \rho E \end{pmatrix}, \quad \mathbf{F}_1 = \begin{pmatrix} \rho u \\ \rho u^2 + P \\ \rho uv \\ uH \end{pmatrix}, \quad \mathbf{F}_2 = \begin{pmatrix} \rho v \\ \rho uv \\ \rho v^2 + P \\ vH \end{pmatrix},$$

$$\mathbf{F}_{1v} = \begin{pmatrix} 0 \\ \tau_{xx} \\ \tau_{xy} \\ -q_x + u\tau_{xx} + v\tau_{xy} \end{pmatrix}, \quad \mathbf{F}_{2v} = \begin{pmatrix} 0 \\ \tau_{yx} \\ \tau_{yy} \\ -q_y + u\tau_{yx} + v\tau_{yy} \end{pmatrix}$$

where *u*, *v*, ρ, *P*, *E*, *H*, τ, and *q* are the *x*-component of velocity, *y*-component of velocity, density, pressure, total energy per unit mass, total enthalpy per unit mass, viscous stresses, and heat flux, respectively; τ and *q* are, respectively, defined by:

$$\tau = (\mu_L + \mu_T)\begin{pmatrix} \frac{4}{3}\frac{\partial u}{\partial x} - \frac{2}{3}\frac{\partial v}{\partial y} & \frac{\partial u}{\partial y} + \frac{\partial v}{\partial x} \\ \frac{\partial u}{\partial y} + \frac{\partial v}{\partial x} & \frac{4}{3}\frac{\partial v}{\partial y} - \frac{2}{3}\frac{\partial u}{\partial x} \end{pmatrix}, \qquad q = k\begin{pmatrix} \frac{\partial T}{\partial x} \\ \frac{\partial T}{\partial y} \end{pmatrix}$$

where μ_L, μ_T, k, and T are the laminar viscosity coefficient, the turbulent viscosity coefficient, the thermal conductivity coefficient, and the temperature, respectively; μ_L is given by the Sutherland formula, and μ_T is given by the SST turbulence model [15].

In eq. (1), $\mathbf{Q} = \partial\mathbf{U}/\partial\mathbf{U}_P$, and $\mathbf{U}_P = (p, u, v, T)^T$. The preconditioning matrix $\mathbf{\Gamma}$ has the form of:

$$\mathbf{\Gamma} = \begin{pmatrix} \theta & 0 & 0 & -\frac{\rho}{T} \\ \theta u & \rho & 0 & -\frac{\rho u}{T} \\ \theta v & 0 & \rho & -\frac{\rho v}{T} \\ \theta H - 1 & \rho u & \rho v & -\frac{\rho(u^2 + v^2)}{2T} \end{pmatrix} \tag{2}$$

where

$$\theta = \frac{1}{a^2 \mathrm{Ma}_r^2} + \frac{\gamma - 1}{a^2} \tag{3}$$

where a and γ are the speed of sound, and the ratio of specific heats, respectively. The Ma_r^2 in eq. (3) is the preconditioning parameter related to the local Mach number. In order to avoid singularities of the preconditioning matrix in the vicinity of stagnation domains Ma_r^2 should be limited and described as [15]:

$$\mathrm{Ma}_r^2 = \min\left[\max(\mathrm{Ma}^2, \sigma \mathrm{Ma}_\infty^2), 1.0\right] \tag{4}$$

where σ is a user-specified constant. It would be advantageous to select this constant to be as small as possible and σ is $1.0 \cdot 10^{-3}$ in this work.

Numerical approach

The advection upstream splitting method (AUSM) meets the goals of efficiency, accuracy and robustness, and is often used in solving high speed flows. The AUSM-family schemes have various developed forms. Liou [15] proposed a new scheme named AUSM$^+$-up for a low Mach number limit, which could be used to solve flows at all speeds. Considering that there are both high speed flow and low speed flow in the computational domain, so the AUSM$^+$-up scheme is used to discretize the convection flux $\mathbf{F}\cdot\mathbf{n}$ in eq. (1). The discretization of $\mathbf{F}\cdot\mathbf{n}$ by the AUSM$^+$-up scheme is described:

$$(\mathbf{F}\cdot\mathbf{n})_{i+1/2} = \dot{m}_{i+1/2}\mathbf{\Phi}_{L/R} + \mathbf{P}_{i+1/2} \tag{5}$$

where $\dot{m}$ is mass flux, $\mathbf{\Phi} = (1, u, v, H)^T$, and $\mathbf{P} = (0, P, 0, 0)^T$. The subscript i+1/2 denotes the interface of cells, L and R represent neighboring grid cells, and $\mathbf{\Phi}_{L/R}$ is defined:

$$\mathbf{\Phi}_{L/R} = \begin{cases} \mathbf{\Phi}_L, & \dot{m}_{i+1/2} > 0 \\ \mathbf{\Phi}_R, & \dot{m}_{i+1/2} \le 0 \end{cases} \tag{6}$$

As the AUSM$^+$-up scheme only has first order accuracy, the monotone upstream-centered scheme for conservation laws (MUSCL) interpolation is adopted in the present study to improve accuracy of the AUSM$^+$-up scheme to second-order accuracy. The viscous flux $\mathbf{F}_v \cdot \mathbf{n}$ in eq. (1) is discretized by the second-order central difference scheme.

The implicit lower-upper symmetric Gauss-Seidel (LU-SGS) scheme has features of high stability, low numerical complexity, and modest memory requirement, which is comparable to an explicit multistage. So the LU-SGS scheme is implemented to discretize the temporal term, which is described and eq. (1) is changed:

$$\Omega \frac{\mathbf{W}^n}{\Delta t} + \mathbf{Q}\mathbf{\Gamma}^{-1} \oint_{\partial Q} [(\mathbf{F}_n - \mathbf{F}_{v,n})^{n+1} - (\mathbf{F}_n - \mathbf{F}_{v,n})^n] \mathrm{d}s = \mathbf{Q}\mathbf{\Gamma}^{-1}\mathbf{R}^n \tag{7}$$

where $\mathbf{W}^n = \Delta\mathbf{U}^n$, $\mathbf{F}_n = \mathbf{F}_1 n_1 + \mathbf{F}_2 n_2$, and $\mathbf{F}_{v,n} = \mathbf{F}_{1v} n_1 + \mathbf{F}_{2v} n_2$. The superscripts n and $n+1$ denote the time level. Hence, $\mathbf{W}^n$ represents the flow solution at the present time, t. Consequently, $\mathbf{W}^{n+1}$ represents the solution at the time $t + \Delta t$. The residual term $\mathbf{R}^n$ has the form:

$$\mathbf{R}^n = \oint_{\partial\Omega} [(\mathbf{F}_n - \mathbf{F}_{v,n})^n \mathrm{d}s \tag{8}$$

Introducing convective flux Jacobians, $\mathbf{A}$, and viscous flux Jacobians, $\mathbf{A}_v$, which are defined as $\mathbf{A} = \partial\mathbf{F}_n/\partial\mathbf{U}$, $\mathbf{A}_v = \partial\mathbf{F}_{v,n}/\partial\mathbf{U}$, eq. (9) becomes:

$$\Omega \frac{\mathbf{W}^n}{\Delta t} + \oint_{\partial\Omega} [\mathbf{A}' - \mathbf{A}'_v]\mathbf{W}^n \mathrm{d}s = \mathbf{Q}\mathbf{\Gamma}^{-1}\mathbf{R}^n \tag{9}$$

where $\mathbf{A}' = \mathbf{Q}\mathbf{\Gamma}^{-1}\mathbf{A}$ and $\mathbf{A}'_v = \mathbf{Q}\mathbf{\Gamma}^{-1}\mathbf{A}_v$. In eq. (11), the convection flux $\mathbf{A}'\mathbf{W}^n$ is discretized by the first-order upstream scheme and viscous flux $\mathbf{A}'_v\mathbf{W}^n$ by the second-order central difference scheme. Hence, eq. (11) becomes:

$$\begin{aligned} &\left[\frac{\Omega}{\Delta t} + \Lambda'_i + \Lambda'_j + 2(\Lambda'_{v,i} + \Lambda'_{v,j})\right]\mathbf{W}^n_{ij} + (\mathbf{A}')^-_{i+1}\mathbf{W}^n_{i+1}\Delta s_{i+1/2} - \\ &-(\mathbf{A}')^+_{i-1}\mathbf{W}^n_{i-1}\Delta s_{i-1/2} + (\mathbf{A}')^-_{j+1}\mathbf{W}^n_{j+1}\Delta s_{j+1/2} - (\mathbf{A}')^+_{j-1}\mathbf{W}^n_{j-1}\Delta s_{j-1/2} - \\ &-\Lambda'_{v,i+1}\mathbf{W}^n_{i+1} - \Lambda'_{v,i-1}\mathbf{W}^n_{i-1} - \Lambda'_{v,j+1}\mathbf{W}^n_{j+1} - \Lambda'_{v,j-1}\mathbf{W}^n_{j-1} = \mathbf{Q}\mathbf{\Gamma}^{-1}\mathbf{R}^n_{ij} \end{aligned} \tag{10}$$

with

$$(\mathbf{A}')^{\pm} = \frac{1}{2}\left[\mathbf{A}' \pm \frac{\Lambda'}{\Delta s}\mathbf{I}\right] \tag{11}$$

where Λ' and Λ'_v are the spectral radius of $\mathbf{A}'$ and $\mathbf{A}'_v$, respectively. Based on eq. (10), the computer code was written in FORTRAN language.

Results

In the simulation, the heat flux, q, on the upstream wall, downstream wall and gap wall were obtained. For the sake of contrastive analysis, the heat flux, q_0, on the flat plat mod-

el without a gap was also computed. The ratio of q/q_0 is shown in fig. 2 and compared with the experimental result from [16].

It can be seen from fig. 2 that the simulation result is consistent with the experimental one, which proves the precision of the model. The heat flux in a gap is U shaped distributed, and decreases rapidly as the increment of depth in a gap. This is because that energy attenuates rapidly as the increment of depth in a gap. Severe high heat flux occurs at the downstream corner of a gap, which should be paid attention in the design of local thermal protection system. Except the area around the entrance of a gap, the heat flux almost equals to zero in the most area of a gap, which illustrates that the external air-flow only affects the local area around the entrance of a gap.

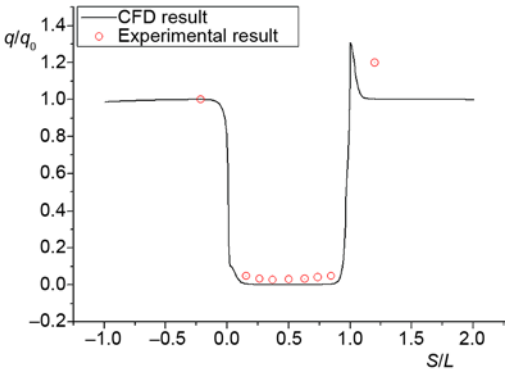

Figure 2. Heating ratio

The temperature contour and streamlines are shown in fig. 3. When the high temperature air in the boundary-layer flows through a gap, it separates from the wall boundary-layer and flows into the gap. As the width of the gap is very small, the separated air collides with the downstream wall of the gap, and then returns to the upstream wall. Under the shear action of the boundary-layer flow, the separated air forms a closed vortex at the entrance of the gap. The vortex is too weak to perturb the gas in the deep area of the gap. In the most are of the gap, the velocity of air-flow almost equals to zero. It can be seen from fig. 3 that the high temperature area only exists at the entrance of a gap, which means the boundary-layer of high temperature has little influence on the deep area in a gap. Based on the flow characteristic and temperature distribution, it can be inferred that the heat convection plays an important role in heat transfer in the gap.

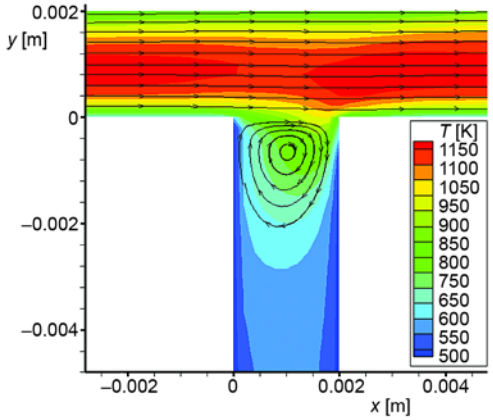

Figure 3. Temperature contour and streamlines (*for color image see journal web site*)

Conclusions

From the numerical results, it can be concluded as follows.

- The heat flux in a gap is U shaped distributed, and severe high heat flux occurs at the downstream corner of a gap, which should be paid attention in the design of local thermal protection system.
- Except a vortex motion exists at the entrance of a gap, the flow velocity in the most area of a gap equals to zero. The heat transfer mechanism in a gap takes the form of heat convection.
- The simulation results are consistent with the experimental ones, which show the viability of the computational method used in this paper.

Acknowledgment

This work is supported by the National Natural Science Foundation of China (11472037 and 11772042) and the opening project of State Key Laboratory of Explosion Science and Technology (BIT, KFJJ15-12M).

Nomenclature

a – speed of sound, [ms^{-1}]
E – total energy per unit mass, [Jkg^{-1}]
H – total enthalpy, [Jkg^{-1}]
k – thermal conductivity coefficient, [Wm^{-1}K^{-1}]
Ma – Mach number, [–]
P – pressure, [Pa]
q – heat flux, [Jm^{-2}s^{-1}]
q_0 – heat flux of flat plate, [Jm^{-2}s^{-1}]
Re – Reynolds number, [–]
T – temperature, [K]
t – time, [s]
u – x-component of velocity, [ms^{-1}]
v – y-component of velocity, [ms^{-1}]

Subcripts

γ – ratio of specific heat coefficient, [–]
μ – dynamic viscosity coefficient, [Pa·s]
ρ – density, [kgm^{-3}]
τ – viscous stresses, [Pa]
Ω – control volume

References

[1] Li, W. J., *et al.*, A Coupled Thermal/Fluid/Chemical/Ablation Method on Surface Ablation of Charring Composites, *International Journal of Heat and Mass Transfer, 109* (2017), Feb., pp. 725-736
[2] Li, W. J., *et al.*, A Nonlinear Pyrolysis Layer Model for Analyzing Thermal Behavior of Charring Ablator, *International Journal of Thermal Science, 98* (2015), Dec., pp. 104-112
[3] Huang, H. M., *et al.*, Numerical Study on Aerodynamic Heat of Hypersonic Flight, *Thermal Science*, *20* (2016), 3, pp. 939 -944
[4] Li, W. J., *et al.*, On the Novel Designs of Charring Composites for Thermal Protection Application in Reentry Vehicles, *Applied Thermal Engineering*, *93* (2016), Feb., pp. 849-855
[5] Li, W. J., *et al.*, Protection of Pyrolysis Gases Combustion against Charring Materials' Surface Ablation, *International Journal of Heat and Mass Transfer*, *102* (2016), Jan., pp. 10-17
[6] Li, W. J., *et al.*, A New Mechanism of Surface Ablation of Charring Materials for a Vehicle during Reentry, *Applied Thermal Engineering*, 106 (2016), Feb., pp. 838-849
[7] Nestler, D. E., *et al.*, Heat Transfer to Steps and Cavities in Hypersonic Turbulent Flow, *AIAA Journal*, *7* (1969), 7, pp. 1368-1370
[8] Menter, F. R., Two-Equation Eddy-Viscosity Turbulence Models for Engineering Applications, *AIAA Journal, 32* (1994), 8, pp. 1598-1605
[9] Avery, D. E., *et al.*, Experimental Aerodynamic Heating to Simulated Shuttle Tiles, *Journal of Spacecraft and Rockets, 22* (1985), 4, pp. 417-424
[10] Dunavant, J. C., *et al.*, Aerodynamic Heat Transfer to RSI Tile Surfaces and Gap Intersections, *Journal of Spacecraft and Rockets, 11* (1974), 6, pp. 437-440
[11] Gartimella, S., *et al.*, Flow and Heat Transfer in Simulated Re-Entry Vehicle Tile Gaps, *Journal of Thermophysics and Heat Transfer, 7* (1993), 4, pp. 644-650
[12] Turkel, E., Preconditioning Techniques in Computational Fluid Dynamics, *Annual Review of Fluid Mechanics, 31* (1999), 1, pp. 385-416
[13] Turkel, E., Preconditioned Methods for Solving the Incompressible and Low Speed Compressible Equation, *Journal of Computational Physics*, *72* (1987), 2, pp. 277-298
[14] Weiss, J. M., *et al.*, Implicit Solution of Preconditioned Navier-Stokes Equation Using Algebraic Multigrid, *AIAA Journal, 37* (1999), 1, pp. 29-36
[15] Liou, M. S., A Sequel to AUSM, Part II: AUSM+-up for All Speeds, *Journal of Computational Physics*, *214* (2006), 1, pp. 137-170
[16] Qian, H. J. *et al. Experimental Study on Heat Flux Distributions in Gaps*, China Academy of Aerospace and Aerodynamics, Beijing, 1996

Paper submitted: January 6, 2017
Paper revised: June 20, 2017
Paper accepted: September 1, 2017